IEEE Robotics and Automation Letters (RA-L) paper, presented at ICRA 2026, Vienna, Austria. Cite as RA-L paper.

IEEE ROBOTICS AND AUTOMATION LETTERS. PREPRINT VERSION. ACCEPTED September, 2025

Autonomous Decentralized Control for Motion Switching in an Intestine-Inspired Peristaltic Mixing Pump Adaptive to Physical Phase Transitions of Mixed Materials

Takaaki Tanno[1], *Student Member, IEEE*, Ryosuke Adachi[1], Koya Tsurumi[1], *Student Member, IEEE*, Fumio Ito[1], *Member, IEEE*, Tomoki Hanamura[2], Takuya Umedachi[2], and Taro Nakamura[1], *Member, IEEE*

***Abstract*— In this paper, we developed an autonomous decentralized control method that incorporates phase-difference adjustment based on a sigmoid function, enabling the design of both increases and decreases in discrepancy. The method was applied to a peristaltic mixing pump capable of mixing and transporting solid–liquid multiphase fluids. This study aims to realize a soft robotics system that autonomously switches motion modes according to changes in the physical properties of the transported material, thereby integratively mimicking both the motility and motion-switching functions of the intestine. Conventional autonomous decentralized control methods have been applied to the locomotion of amoeba-type and snake-type robots. However, when such control laws are applied to pumps, it is difficult to achieve appropriate motion switching in environments where the contents harden due to mixing. In this paper, we employed a sigmoid function that allows bidirectional control of discrepancy and constructed a new control law based on target phase-difference adjustment without feedback. The control law was implemented in a four-unit pump, and we confirmed that the desired motion patterns could be reproduced according to the preset target phase differences. As a result, the phase differences between all units converged to the target values within approximately 10–30 s after actuation began, producing the intended motion patterns. Furthermore, polyvinyl alcohol solution and borax water were used as contents whose fluidity decreases during mixing. We verified that autonomous motion switching occurred as the discrepancy increased. The results showed that, in units containing hardened material, a conveying motion with a phase difference of $\pi/3$ was generated, whereas in units with residual unmixed material, a mixing motion with a phase difference of π was generated. These findings demonstrate that the proposed method enables motion control that adapts to changes in material properties.**

I. Introduction

The intestine's motility is controlled by the central and enteric nervous systems. The enteric system, containing sensory and interneurons, has reflex circuits that determine motion patterns in response to mechanical and chemical stimuli without brain input [1–3]. Main motions are peristalsis for transport, segmentation for mixing, and pendular motion [4]. The flexible wall allows low-shear mixing and transport of high-viscosity, solid–liquid multiphase fluids. Pumps modeled on these motions and switching control can achieve continuous, efficient mixing and transport, enabling more efficient food and pharmaceutical manufacturing.

Previous studies using neural oscillator–based intestinal models confirmed motion generation in simulations with varying content hardness [5–7] and achieved autonomous peristalsis in swallowing devices [8–10]. These were limited to idealized simulations or single motion sequences, and no autonomous decentralized control method could switch motions for materials that harden during mixing. Intestine-mimicking pumps with pneumatic artificial muscles [11][12] also used sequence control, making adaptation to property changes difficult. Real hardware requires control that reflects real-time fluidity and state changes.

In previous work, we developed a peristaltic mixing pump [13] with connected, air-occludable tubes. Using sequence control with a single microcontroller, we mixed and transported high-viscosity fluids and powders [14][15]. However: (1) the control law required modification when the number of units changed; (2) all units followed the same pattern, making adaptation to mixing-state changes difficult. Fixed-time sequence control risks quality loss from under-mixing or efficiency loss from over-mixing. Thus, a control system that autonomously adapts motion patterns to property changes is needed.

This study aims to establish a control law for a peristaltic mixing pump based on autonomous decentralized control, enabling motion switching according to the state of the contents.

We focused on local feedback control based on a discrepancy function, used in snake-type [16] and amoeba-type robots [17], where joint angle or spring length was treated as phase. For pumps, phase was defined as the unit's air-supply state, and discrepancy as the difference between integrated and no-load airflow [18]. Implementing this method enabled switching from mixing to peristalsis as fluidity increased [19]. However, as in Kano et al. [7], it was difficult to generate peristalsis when discrepancy increased, such as with hardening contents that hinder occlusion. This limits applications to gels, jams, and polymer–additive mixtures in pharmaceuticals and cosmetics. A phase-adjustment method that responds to both increases and decreases in discrepancy is needed.

Manuscript received: April 30, 2025; Revised: August 9, 2025; Accepted: August 31, 2025.

This paper was recommended for publication by Editor Cecilia Laschi upon evaluation of the Associate Editor and Reviewers' comments.

[1]T. Tanno, R. Adachi, K. Tsurumi, F. Ito, and T. Nakamura are with the Department of Precision Mechanics, the Faculty of Science and Engineering, Chuo university, 1-13-27 Kasuga, Bunkyo-ku, 112-8551 Tokyo, Japan (Corresponding author e-mail: t_tanno@bio.mech.chuo-u.ac.jp).

[2]T. Hanamura and T. Umedachi are with the Department of Mechanical Engineering and Robotics, Faculty of Textile Science and Technology, Shinshu university, 3-15-1 Tokida, Ueda City 386-8567 Nagano, Japan.

Digital Object Identifier (DOI): see top of this page.

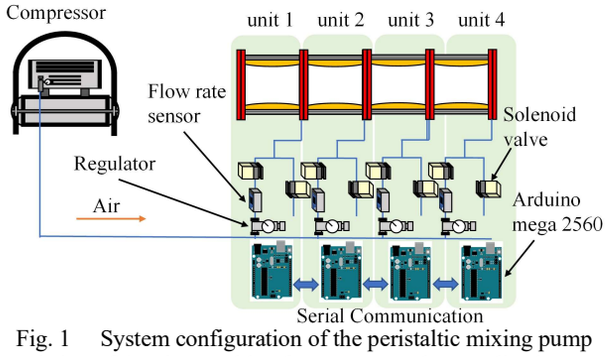

Fig. 1 System configuration of the peristaltic mixing pump consisting of 4-units capable of autonomous decentralized control

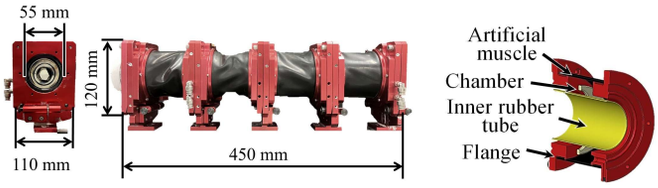

(a) External view of the 4-unit pump (b) Detailed structure of one unit

(c) Occlusion mechanism of the inner rubber tube through pneumatic actuation

Fig. 2 Structure and appearance of the peristaltic mixing pump

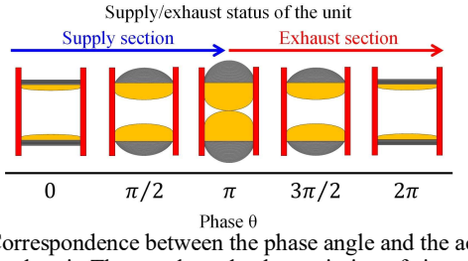

Fig. 3 Correspondence between the phase angle and the actuation state of each unit. The supply and exhaust timing of air pressure is mapped to specific ranges of the unit phase θ.

In this paper, we propose a control law linking the discrepancy function—defined by inter-unit phase difference and integrated airflow—to a sigmoid function, applied to multi-unit pumps. This enables autonomous switching according to fluidity changes, uniquely determining target phase difference and handling both increase and decrease in discrepancy. We first verify phase-difference-only control in a four-unit pump, then test the sigmoid-based method with contents whose fluidity decreases during mixing, confirming switching from mixing to peristalsis. The contributions are:

– Development of an autonomous decentralized control law using sigmoid-based phase adjustment for adaptive motion switching under material property changes.

– Experimental demonstration of autonomous transition to peristalsis in contents with increasing viscosity, which conventional local feedback control cannot handle.

– Indication of applicability to adaptive motion control in soft robotics under diverse environments.

The structure of this paper is as follows. Section 2 outlines the autonomous decentralized control system of the peristaltic mixing pump. Section 3 presents the general form of the conventional control law and explains the proposed sigmoid function–based control law. Section 4 describes experiments verifying motion generation based on a set phase difference, and Section 5 presents experiments verifying motion switching according to changes in content state using the sigmoid function.

II. Autonomous Decentralized Motion Control System for Peristaltic Mixing Pump

This section describes the autonomous decentralized control system for a peristaltic mixing pump developed to emulate biological intestinal motion and its pattern-switching mechanisms. First, the overall system configuration is outlined. Then, the structure and operating principles of the pump, designed to replicate intestinal motility, are explained.

A. System Configuration

The system configuration is illustrated in Fig. 1. Each unit of the pump is supplied with compressed air through an air circuit equipped with two solenoid valves (SMC VDW20JA) for air intake and exhaust, and two flow sensors (SMC PEM750-C6-C) for measuring the intake and exhaust flow rates. Compressed air for driving the pump is supplied by an air compressor, and the pressure is regulated using a pressure regulator. The opening and closing of the solenoid valves and the acquisition of flow rate data in each unit are controlled by a microcontroller (Arduino MEGA 2560). Microcontrollers can exchange information with neighboring units via serial communication.

B. Pump Overview

An external view of the pump is shown in Fig. 2(a). The pump consists of multiple interconnected units, each structured as shown in Fig. 2(b). Each unit comprises an outer axially fiber-reinforced pneumatic artificial muscle (hereafter referred to as an "artificial muscle") and an inner rubber tube, which are joined together via flanges. The pump operates by applying pneumatic pressure to the chamber space between the artificial muscle and the rubber tube. This causes the rubber tube to expand inward, occluding the lumen, while the artificial muscle expands radially outward and contracts axially. The combined effect of axial contraction and lumen occlusion pushes the contents within the unit, enabling mixing and transport through the tube. Furthermore, by controlling the timing of air intake and exhaust for each unit, the pump can replicate intestinal motion.

In this study, two motion patterns realizable by the pump are defined: peristaltic motion and mixing motion. Peristaltic motion refers to the transport of contents in a specific direction. In this mode, when a unit extends due to exhaust, adjacent units grasp the contents to prevent backflow, thereby enabling

unidirectional transport. Thus, achieving peristaltic motion requires appropriately staggered air control timing between adjacent units. Here, when the supply and exhaust states of each unit are expressed using the phase θ ($0 \leq \theta \leq 2\pi$) shown in Fig. 3, an ideal peristaltic motion is defined as a state in which three or more adjacent pump units operate with a constant intrinsic phase difference ω and maintain it. In this study, considering the pneumatic response of the pump, peristaltic motion is defined as the condition in which the phase difference between three or more adjacent units, $\theta_{i+1} - \theta_i$ (i: unit index), converges to $\omega \pm \pi/6$ and is maintained for at least 30 s. If these conditions are not met, the contents are mixed regardless of the pump's motion pattern, and this state is defined as mixing motion.

III. Control Law Design

A. General formula for Autonomous Decentralized Control

First, the general form of the decentralized autonomous control law, which has been adapted for the motion control of modular robotic units, is presented in Equation (1).

$$\frac{d\theta_i}{dt} = \omega + F(\theta_{i-1}, \theta_i, \theta_{i+1}) \tag{1}$$

The subscript i corresponds to the unit number, with unit 1 located on the content inlet side, and the index increasing by one toward the outlet. The variable θ_i ($0 \leq \theta_i \leq 2\pi$) represents the phase of unit i , corresponding to the unit's air supply and exhaust state, as illustrated in Fig. 3. The first term ω, denotes the natural frequency, and the second term, $F(\theta_{i-1}, \theta_i, \theta_{i+1})$, is a phase adjustment term. In conventional control laws, $F(\theta_{i-1}, \theta_i, \theta_{i+1})$ consists of two components: a phase difference setting term to synchronize the motions of adjacent units, and a local feedback term based on discrepancy detection. In contrast, the control law proposed in this study adopts only the phase difference setting term and does not use any local feedback term. In the following, the conventional control law is first outlined, followed by a detailed description of the proposed control law based on sigmoid-function-driven phase difference adjustment.

B. Previous Method: Control using Local Feedback Terms [16][17]

$$F(\theta_{i+1}, \theta_i, \theta_{i-1}) = f(\theta_{i-1}, \theta_i, \theta_{i+1}) + g(\theta_i) \tag{2}$$

$$f(\theta_{i-1}, \theta_i, \theta_{i+1}) = \epsilon(\sin(\theta_{i+1} + \theta_i + \psi_i) + \sin(\theta_{i-1} - \theta_i - \psi_i)) \tag{3}$$

$$g(\theta_i) = -\partial I_i(\theta_i)/\partial\theta_i \tag{4}$$

$$I_i(\theta_i) = \frac{\sigma}{2}{T_i}^2 \tag{5}$$

This section describes control laws previously applied to snake-like robots [16] and amoeba-like robots [17]. In these methods, the second term of Equation (1) is expressed as the sum of $f(\theta_{i-1}, \theta_i, \theta_{i+1})$ and $g(\theta_i)$, as shown in Equation (2).

Equation (3) represents a diffusive interaction between adjacent phase-difference oscillators, designed to pull them toward the target phase difference ψ_i. Such synchronization control using a phase-difference setting term is a basic method in nonlinear dynamics for achieving stable phase-difference synchronization. It is generally known that increasing the control gain ε broadens the range of acceleration differences over which entrainment occurs [21].

Meanwhile, $g(\theta_i)$ is a local feedback term that adjusts the unit's phase based on the discrepancy calculated from its deformation. The discrepancy is defined as the difference between the actual deformation and its target value, expressed as an energy function $I_i(\theta_i)$. By adjusting the acceleration in the direction of the negative gradient of this function (Eqs. (4) and (5)), the discrepancy is reduced. This allows the control system to adapt to mechanical loads such as friction, flexibly modifying the phase evolution speed of each unit and generating motions that the entire system can perform without excessive load [22].

Thus, the control law consists of two layers: a structurally stable phase-difference setting term and a local feedback term robust to environmental variations. This structure enables stable and adaptive operation even in real environments with disturbances such as changes in material properties of the contents. Moreover, since each unit is controlled using only local interactions with its neighbors, the control structure and computational load remain simple as the number of units increases, ensuring high scalability.

This control law has been applied and validated in various platforms, including taxis and exploratory behaviors of amoeba-type soft robots [17][23][24], serpentine locomotion of snake-type robots adapted to frictional environments [16], and gait transitions of quadruped robots according to speed [25]. In all these robotics applications, robustness to environmental changes and stability of motion were confirmed.

This study applies a similar control law to an intestine-mimicking pump. In the previous work by Tsurumi et al. [19], the control was designed so that $f(\theta_{i-1}, \theta_i, \theta_{i+1})$ dominated when the pump units could push the contents without excessive load, and $g(\theta_i)$ dominated when mixed contents prevented the units from pushing them out. This design enabled autonomous switching from mixing to conveying for contents whose fluidity increased during mixing.

However, when fluidity decreases during mixing and discrepancy increases, control dominated by the phase-difference setting term $f(\theta_{i-1}, \theta_i, \theta_{i+1})$ becomes difficult, hindering the transition to peristaltic motion. Therefore, the next section proposes a new sigmoid function–based autonomous decentralized control law that adaptively adjusts the phase difference in response to both increases and decreases in discrepancy.

C. Proposed Method: Control Applying the Sigmoid Function

$$\frac{d\theta_i}{dt} = \omega + F(\theta_{i-1}, \theta_i, \theta_{i+1}, \psi_i, \psi_{i-1}) \tag{6}$$

$$F(\theta_{i-1}, \theta_i, \theta_{i+1}, \psi_i, \psi_{i-1}) = \epsilon(\sin(\theta_{i+1} - \theta_i + \psi_i) + \sin(\theta_{i-1} - \theta_i - \psi_{i-1})) \tag{7}$$

$$\psi_i(S_{j_i}) = \frac{A}{1 + e^{S_{j_i} - B}} + C \quad (j_i = 1,2,\cdots) \tag{8}$$

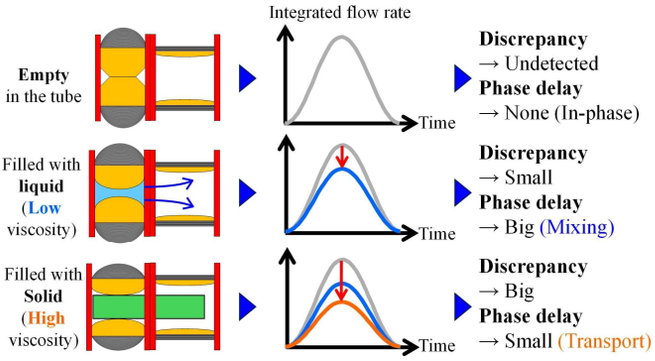

Fig. 4 Effect of differences in contents on chamber integrated flow rate, discrepancy, and phase delay

$$S_{j_i} = \int_{\tau_{j_{i-2}}}^{\tau_{j_{i-1}}} {I_i}^2 dt \quad (j_i = 1,2,\cdots) \tag{9}$$

$$T_i = Q_i - Q_{cmd} \tag{10}$$

$$Q_{cmd} = n(1 - \cos\theta_i) \tag{11}$$

This section explains the proposed control law using a sigmoid function. In this law, Eq. (6) is obtained by adding the target phase differences ψ_i and ψ_{i-1} to the second term $F(\theta_{i-1}, \theta_i, \theta_{i+1})$ in Eq. (1). The value of ψ_i is then varied according to the discrepancy function, as in Eq. (7), enabling phase-difference control based on the state of the contents. Here, ψ_{i-1} refers to the phase difference with the unit on the side opposite to the conveying direction. Aligning the phase differences with both neighboring units helps maintain a constant phase difference across all units, contributing to stable generation of peristaltic motion.

In decentralized control systems, nonlinear functions such as Gaussian [26–28] and sigmoid functions [29][30] are commonly used to map input values to control parameters. The sigmoid function, in particular, offers a smooth transition from 0 to 1, continuous and monotonic response over a wide input range, and low computational cost, making it suitable for the autonomous decentralized control of this pump, where real-time performance and smooth control are required. Accordingly, in the proposed control law, as shown in Eqs. (8) and (9), the target phase difference ψ_i is determined by applying the sigmoid function to the integrated value $S_{ji}(\theta_i)$ of the discrepancy function $I_i(\theta_i)$ over one supply–exhaust cycle ($0 \le \theta_i \le 2\pi$). By adjusting constants A, B, and C in Eq. (8), the system is designed to select an appropriate motion pattern (mixing or conveying) according to changes in content fluidity. In Eq. (8), the subscript j_i of S_{ji} denotes the cycle number, starting from $j_i = 1$ at the beginning of pump operation, and τ_{ji} represents the end time of the j_i-th cycle.

Differences in airflow into each pump unit correspond to changes in the fluidity of the contents [18]. Therefore, the discrepancy T_i, which determines the phase control of each unit, is expressed in Eq. (10) as the difference between the commanded integrated airflow Q_{cmd} and the measured integrated airflow Q_i. Q_{cmd} is calculated from Eq. (11) using the command amplitude n and phase θ_i assigned to each unit. This equation is an approximate function derived from the integrated airflow response when the tube is occluded with no contents inside.

Next, we explain how the proposed control law detects discrepancy caused by content fluidity and adjusts the phase accordingly. As shown in Fig. 4, the time-series response of integrated airflow into a unit varies with the tube's state (empty, liquid-filled, or solid-filled). When empty, air flows easily into the chamber, and the integrated airflow increases rapidly. When filled with liquid, flow resistance slows the response. When filled with high-viscosity solids, the contents occlude the tube, greatly restricting airflow and resulting in much lower integrated values than in the empty state. These differences in airflow response are reflected in the unit's discrepancy T_i, producing variations in phase lag and mismatch. In the proposed sigmoid function–based control law, the target phase difference ψ_i is adjusted according to changes in discrepancy, enabling autonomous switching of motion patterns in response to changes in content properties.

IV. Motion Pattern Generation Experiment Using Target Phase Difference Adjustment [16]

This chapter describes experiments applying the control law given by Eqs. (6) and (7) in Section 3.C to the pump, verifying that the desired motion pattern can be generated according to preset target phase differences ψ_i and ψ_{i-1}. These experiments confirm that the pump's motion pattern can be changed solely by adjusting the target phase differences, without using the local feedback term employed in conventional control methods.

A. Experiment Overview

$$F(\theta_{i-1}, \theta_i, \theta_{i+1}, \psi_i) = \epsilon(\sin(\theta_{i+1} - \theta_i + \psi_i) + \sin(\theta_{i-1} - \theta_i - \psi_i)) \tag{12}$$

The experimental setup was the same as the system configuration shown in Fig. 1. The applied pressure to each unit was 30 kPa, the sampling period of the flow sensor was 50 ms, and the command amplitude n for integrated airflow was set individually according to the air supply capacity of each unit. The natural frequency ω was $\pi/3$ rad/s, and each unit operated in a 6 s cycle of 3 s supply and 3 s exhaust. The feedback gain ε for the phase-difference setting term was 0.03, and the total pump operation time was 60 s. The target phase differences ψ_i were set to 0, $\pi/3$, π, and $5\pi/3$. To evaluate pump behavior when the same target phase difference was set for all units, Eq. (12), a simplified form of Eq. (7), was used, with $\psi_{i-1} = \psi_i$ to unify the target phase difference for all units. During operation, an acrylic pipe (φ = 30 mm, length = 550 mm) was placed inside the rubber tube to be driven by the generated motion.

The expected motions for each target phase difference condition are as follows. When $\psi_i = 0$, all units operate in phase, supplying and exhausting air simultaneously. When $\psi_i = \pi/3$, the supply–exhaust timing between adjacent units differs by 1 s, producing peristaltic motion in which the tube is occluded sequentially from the unit with the smallest index i. When $\psi_i = \pi$, the timing differs by 3 s, causing adjacent units to alternately supply and exhaust air, which is expected to generate mixing motion. When $\psi_i = 5\pi/3$, each unit's phase development lags 5 s behind that of the adjacent unit with index $i-1$, producing peristaltic motion in the opposite direction to that for $\psi_i = \pi/3$.

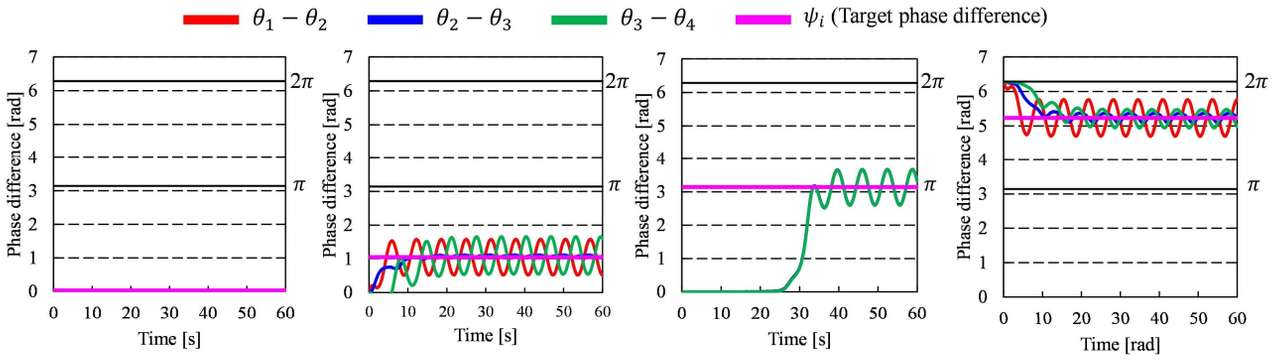

(a) $\psi_i = 0$ (b) $\psi_i = \pi/3$ (c) $\psi_i = \pi$ (d) $\psi_i = 5\pi/3$

Fig. 5 Measured time-series transitions of phase differences between adjacent units under different target phase difference conditions (ψ_i). Four graphs correspond to different target values.

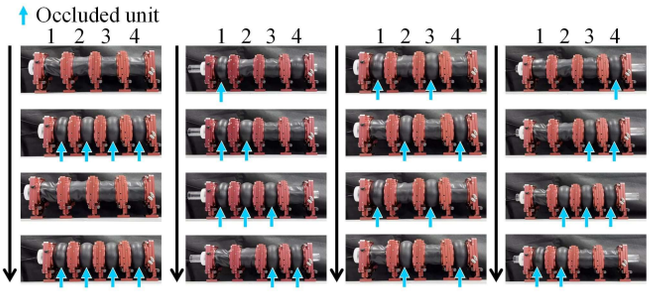

(a) $\psi_i = 0$ (b) $\psi_i = \pi/3$ (c) $\psi_i = \pi$ (d) $\psi_i = 5\pi/3$

Fig. 6 Motion transitions of the pump under different target phase differences. Each image shows the occlusion states of the units over time. Cyan arrows indicate units with closed chambers due to pneumatic actuation.

B. Experimental Results and Discussion

The experimental results are shown in Figs. 5 and 6. Fig. 5 presents the time-series changes in phase differences between units for each target phase difference, and Fig. 6 shows the pump operation under each condition.

For ψ_i = 0, Fig. 5 (a) shows that the phase differences between units remained at 0, and Fig. 6 (a) confirms that all four units supplied and exhausted air in synchrony for 60 s.

For ψ_i = π/3, Fig. 5 (b) shows that the units were synchronized for the first 5 s, after which phase differences gradually developed and converged to π/3 by 10 s. Fig. 6 (b) shows air supplied sequentially from Unit 1 to Unit 4, generating rightward peristaltic motion.

For ψ_i = π, Fig. 5 (c) shows that all units operated in phase until 25 s, after which the phase differences gradually increased and converged to π at around 32 s. Fig. 6 (c) shows that after 26 s, Units 1 and 2 alternated supply and exhaust with Units 3 and 4, generating segmentation motion.

For ψ_i = 5π/3, Fig. 5 (d) shows that variations in phase evolution speed appeared after 2 s, and the phase differences converged to π/3 by 10 s. Fig. 6 (d) confirms leftward peristaltic motion from Unit 4 to Unit 1.

These results show that the expected motions were generated for all target phase differences. However, while ψ_i = π/3 and 5π/3 required about 10 s for phase convergence, ψ_i = π showed no phase difference until 26 s and required 32 s to converge. To examine the cause of this delay, letting $\theta_{i+1} - \theta_i = A$ and $\theta_{i-1} - \theta_i = B$, Eq. (12) can be expanded using the addition theorem to yield Eq. (13).

$$F(\theta_{i-1}, \theta_i, \theta_{i+1}, \psi_i) = \epsilon \sin A \cos\psi_i + \epsilon \cos B \sin\psi_i + \epsilon \sin B \cos\psi_i - \epsilon \cos A \sin\psi_i \quad (13)$$

Here, when ψ_i = π, sin ψ_i = 0. At the start of operation, the phase differences are small, so sin A and sin B are also nearly zero, resulting in F ≈ 0 and little phase evolution. This likely caused the delayed phase convergence.

In summary, implementing the control law based solely on target phase-difference adjustment in the pump demonstrated the ability to generate specified motion patterns. Introducing target phase-difference adjustment responsive to discrepancy changes into this control law is expected to enable motion control according to both increases and decreases in discrepancy without using a local feedback term. The next chapter describes experiments verifying autonomous motion pattern switching using the extended control law with sigmoid-based phase-difference adjustment.

V. Motion Switching Experiments Based on Sigmoid Function

This chapter describes experiments applying the control law with sigmoid-based phase-difference adjustment to the pump for autonomous decentralized control. The experiments verify whether the motion pattern autonomously transitions to peristaltic motion under conditions where content fluidity decreases during mixing.

A. Experiment Overview

The experimental setup was the same as that shown in Fig. 1. The applied pressure, flow sensor sampling period, commanded integrated airflow amplitude n, natural frequency ω, feedback gain ε for the phase-difference setting term, and total pump operation time were set as in Chapter 4. Based on preliminary experiments with the pump operating in an empty state, the constants in the sigmoid function of Eq. (7) were set to A = 2π/3, B = 26, and C = π/3.

The mixing materials were 200 mL of commercial polyvinyl alcohol (PVA) laundry glue and 100 mL of borax solution prepared by dissolving 5 g of borax in 100 mL of

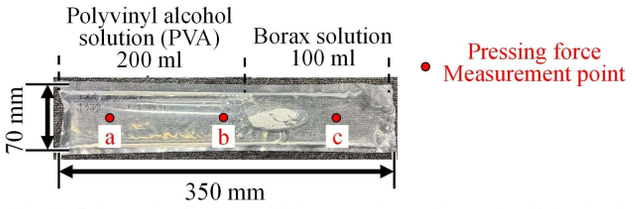

Fig. 7 Schematic diagram of the experimental sample (Polyvinyl alcohol (PVA) solution and borax solution) and pressing force measurement points

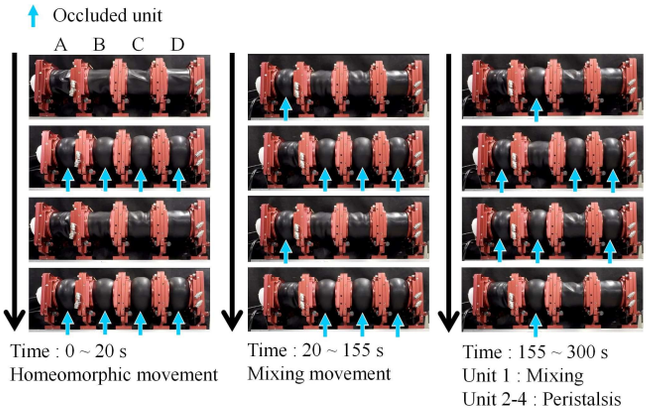

Fig. 8 Time-lapse visualization of the pump's motion pattern during the experiment, showing the cyclic occlusion and release of each unit. (1st trial)

water. Each was sealed in a polyethylene bag (70 × 350 mm). When loaded into the pump, the PVA was positioned on the Unit 1 side, as shown in Fig. 7.

To evaluate changes in content hardness before and after mixing, each bag was compressed with a force gauge (Measurement section area: φ12 mm) to measure the maximum compression force. Measurements were taken three times at each of three points (a, b, and c in Fig. 7). Comparing the forces before and after mixing allowed quantitative evaluation of hardness changes caused by the pump's mixing.

When PVA and borax solution are mixed, a cross-linking reaction occurs between PVA molecules and borate ions, increasing viscosity through gelation. In the initial stage, high fluidity prevents occlusion from being hindered, resulting in small discrepancy and generation of mixing motion. As mixing progresses, gelation reduces fluidity and makes occlusion difficult, increasing discrepancy and causing the motion pattern to autonomously shift to peristaltic motion.

To verify the reproducibility of motion switching, three pump operation trials were conducted with the contents loaded. Hardness evaluation by compression force measurement was performed in two of these trials.

In this experiment, $\omega = \pi/3$ [rad/s]. According to the definition of peristaltic motion in Section 2.B, the convergence condition for peristaltic motion is that the phase differences θ_{i+1}-θ_i of at least three out of the four units converge to $\pi/6 \leqq \theta_{i+1}$-$\theta_i \leqq \pi/2$ and remain in this range for at least 30 s.

B. Experimental Results and Discussion

From video recordings of the first trial, the pump operation at different times is shown in Fig. 8. For the first 20 s after startup, all units operated in phase. From 20 to 155 s, the units supplied and exhausted air at different timings, producing a random mixing motion. After 155 s, Units 2–4 maintained peristaltic motion, while Unit 1 continued mixing motion with a different phase. However, inspection of the mixed sample revealed that the hardened material was not concentrated on the Unit 4 side but remained as small lumps scattered within the bag.

Fig. 9 visualizes the phase changes of each unit in the first trial using a gradient from white (0 rad) to black (2π rad). Each unit is assigned a different gradient color (red: Unit 1, blue: Unit 2, green: Unit 3, yellow: Unit 4). One stripe represents a single supply–exhaust cycle, and the offset between stripes indicates the phase difference between adjacent units. The results show that until 20 s, there was no offset, indicating in-phase motion. From 20 to 155 s, stripe offsets appeared, and all units operated at different timings, producing mixing motion. After 155 s, the stripes of Units 2–4 were arranged at regular intervals, indicating peristaltic motion, while the phase difference between Units 1 and 2 increased, showing that Unit 1 continued independent mixing motion.

Fig. 10 shows the time variation of phase differences between adjacent units for all three trials. The horizontal axis indicates time from the start of operation, and the vertical axis shows the phase difference between adjacent units. In all trials, the phase differences were near zero immediately after startup. After 10 s, phase differences began to develop in the order θ_2-θ_3, θ_1-θ_2, and θ_3-θ_4, producing mixing motion. In Trial 1, at 155 s, in Trial 2 at 203 s, and in Trial 3 at 283 s, both θ_2-θ_3 and θ_3-θ_4 reached the convergence condition for peristaltic motion, confirming a transition to peristaltic motion in Units 2–4. In contrast, θ_1-θ_2 converged to π rad in all trials, indicating that Unit 1 continued mixing motion throughout. These results confirm that the transition from mixing to peristaltic motion occurred in all trials, demonstrating the reproducibility of motion switching with the proposed control law.

Fig. 11 shows the maximum compression force measurements before and after mixing for Trials 2 and 3. In both trials, the maximum compression force increased at all measurement points, quantitatively confirming hardening of the contents. In Trial 2, the increase was largest in the order *c*, *b*, and *a* from the borax solution side. In Trial 3, the largest increase occurred at the central point *b*, with smaller increases at *a* and *c*.

From the above, the motion pattern changes of the pump can be interpreted as follows. For the first 20 s, the high fluidity of the contents allowed unobstructed occlusion, and all units operated in phase. After 20 s, occlusion in the tube caused the low-viscosity borax solution to flow toward and mix with the PVA on the Unit 1 side, producing hardened material. This likely hindered occlusion in Units 1 and 2, increasing discrepancy and thus increasing θ_2-θ_3 and θ_1-θ_2.

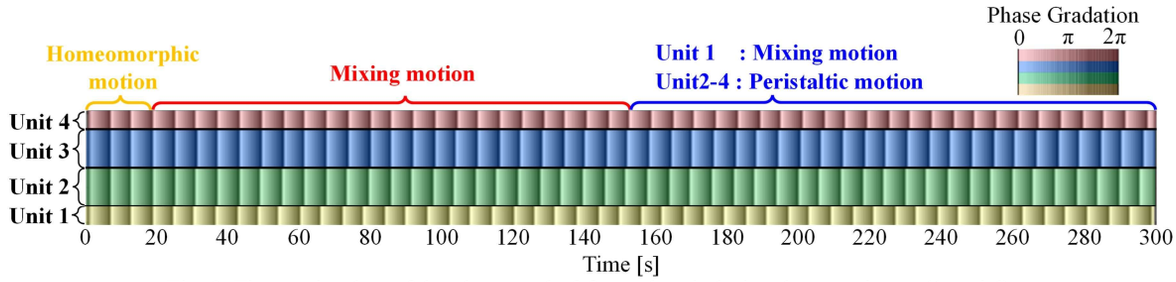

Fig. 9 Time series data of the phase angle θ for each unit during the experiment (1st trial)

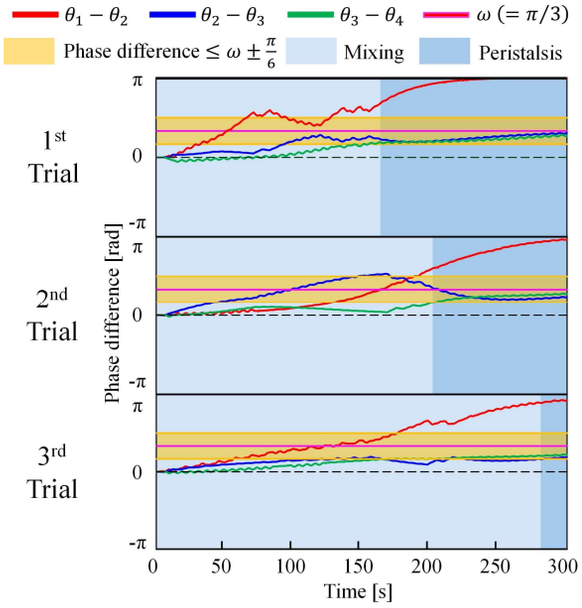

Fig. 10 Time-series transition of phase differences between adjacent units and visualization of motion switching

Subsequently, hardening also progressed on the Unit 4 side due to mixing of borax solution and PVA, which likely caused θ_3-θ_4 to begin increasing in the same manner.

Next, in Units 2–4, continued discrepancy increase due to the hardened mixture, combined with the action of the sigmoid function linked to ψ_i, likely caused θ_2-θ_3 and θ_3-θ_4 to shift toward convergence at ω (=π/3), resulting in peristaltic motion in these units. In contrast, the PVA in Unit 1 had higher viscosity than the borax solution, and even after mixing motion was generated, part of the PVA likely remained in the unit. This would have limited the increase in discrepancy, causing Unit 1 to maintain mixing motion until the end, with its phase difference converging toward π.

In Trial 3, the transition to peristaltic motion took longer than in Trials 1 and 2. This is presumed to be due to significant hardening of the contents near Unit 2, which occluded the tube and restricted solution flow. As a result, mixing progressed more slowly, leaving unmixed regions at the ends of the bag. Consequently, as shown in Fig. 11(b), the changes in compression force at points *a* and *c* near the bag ends were smaller than at point *b* in the center.

Another possible reason the contents were not fully transported to the Unit 4 side by the peristaltic motion of Units 2–4 is that the occlusion actions may have caused the hardened mixture to break apart, making continuous gripping

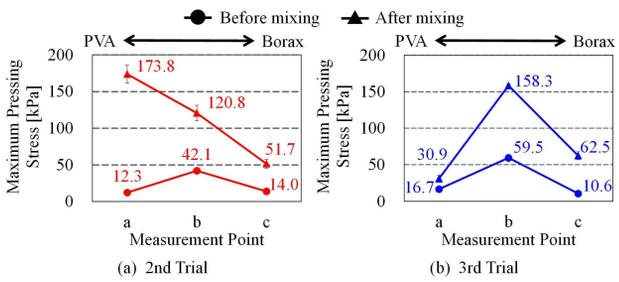

Fig. 11 Comparison of maximum pressing force at each measurement point before and after mixing in the 2nd and 3rd trials

and transport, as with a rigid rod, difficult. This likely led to uneven distrib ution of the contents and resulting bias in the measured changes in compression force.

C. General Discussion

These experiments confirmed that the proposed autonomous decentralized control law using a sigmoid function can autonomously switch from mixing to peristaltic motion in response to changes in content properties. The phase difference was adjusted according to discrepancy changes caused by hardness variation during mixing, and reproducible motion switching was observed in all three trials. In particular, the phase differences of Units 2–4 converged to π/6–π/2, generating peristaltic motion, while Unit 1 converged to π due to residual unmixed PVA, resulting in continued mixing motion.

These results demonstrate that the proposed method enables phase synchronization even when discrepancy increases—a capability difficult to achieve with conventional local feedback control [19]—and thus contributes to expanding the applicability of autonomous decentralized control methods in soft robotics to diverse environmental changes.

As a remaining challenge, partial hardening or breakage of the mixture made continuous transport difficult, causing the contents to stagnate. To address this, future work will use machine learning based on pressure, flow rate, and other measurements to estimate material properties in detail, and adaptively control parameters such as applied pressure, operating frequency, and feedback gain to improve robustness and mixing–transport efficiency. In addition, since the nonlinear function type and sigmoid parameters in this study were selected empirically, future work will also consider selecting functions based on material properties and optimizing parameters using the aforementioned machine learning approach.

Furthermore, although this study verified the performance

of the control law using only PVA and borax solution, future work will evaluate the proposed method with different types and compositions of contents, and quantitatively compare it with existing methods in terms of motion transition time, mixing rate, and energy efficiency. In addition, fluid–structure interaction (FSI) simulations and theoretical validation based on physical modeling of the contents will be conducted to further develop the control law for broader applicability.

VI. Conclusion

This study proposed an autonomous decentralized control law using a sigmoid function, enabling autonomous switching from mixing to peristaltic motion for mixed materials with changing properties. Experiments with PVA and borax solution showed that the phase difference was appropriately adjusted according to discrepancy changes caused by hardening, and reproducible motion switching was achieved. The method enabled phase synchronization during discrepancy increase—a challenge for conventional local feedback control—demonstrating its effectiveness as a control approach adaptable to diverse physical changes.

References

[1] J. B. Furness, et al., " The Enteric Nervous System and Gastrointestinal Innervation: Integrated Local and Central Control," Microbial Endocrinology: The Microbiota-Gut-Brain Axis in Health and Disease, pp. 39-71, Jul. 2014.

[2] R. K. Goyal and I. Hirano, "The Enteric Nervous System," The New England Journal of Medicine vol.334, no.17, pp. 1106-1115, Apr. 1996.

[3] M. B. Hansen and A.-B. Witte, "The role of serotonin in intestinal luminal sensing and secretion," Acta Physiologica vol. 193, issue 4, pp. 311-323, Jul. 2008.

[4] H. M. Cheng, et al., "Motility: Peristalsis, Segmentation, Haustration and Mass Movement," Defining Physiology: Principles, Themes, Concepts. Volume 2 Neurophysiology and Gastrointestinal Systems, pp. 35-37, 2020

[5] E. A. Thomas, et al., "A computational model of the migrating motor complex of the small intestine," American Journal of Physiology Gastrointestinal and Liver Physiology vol. 286, issue 4, pp. 564-572, Apr. 2004.

[6] S. Kuruppu, et al., "High-Resolution Spatiotemporal Quantification of Intestinal Motility With Free-Form Deformation," IEEE Transactions on Biomedical Engineering vol. 69, issue 6, pp. 2077-2086, Dec. 2021.

[7] T. Kano, et al., "Generating Situation-Dependent Behavior: Decentralized Control of Multi-Functional Intestine-Like Robot that can Transport and Mix Contents," Journal of Robotics and Mechatronics vol. 25, no. 5, pp. 871-876, Oct. 2013.

[8] S. Dirven, et al., "Sinusoidal Peristaltic Waves in Soft Actuator for Mimicry of Esophageal Swallowing," IEEE/ASME Transactions on Mechatronics vol. 20, no. 3, pp. 1331-1337, Jun. 2015.

[9] S. Din, et al., "A Stretchable Array of Electronic Receptors for Esophageal Swallowing Robot for Biomimetic Simulations of Bolus Transport," IEEE Sensors Journal vol. 18, no.13, pp. 5497-5506, Jul. 2018.

[10] M. Zhu, et al., "Esophageal Peristaltic Control of a Soft-Bodied Swallowing Robot by the Central Pattern Generator," IEEE/ASME Transactions on Mechatronics vol. 22, issue 1, pp.91-98, Sep. 2016.

[11] Y. Peng, et al., "Peristaltic transporting device inspired by large intestine structure," Sensors and Actuators A: Physical, vol. 365, Jan. 2024.

[12] Y. Peng, et al., "Controlling a peristaltic robot inspired by inchworms," Biomimetic Intelligence and Robotics, vol. 4, issue 1, Mar. 2024.

[13] K. Suzuki and T. Nakamura, "Development of a peristaltic pump based on bowel peristalsis using for artificial rubber muscle," in: Proceedings of the 2010 IEEE/RSJ International Conference on Intelligent Robots and Systems (IROS2010), Taipei, Republic of China, 2010, pp. 3085-3090.

[14] S. Yoshihama, et al., "Mixing of solid propellant by peristaltic pump based on bowel peristalsis," in: Proceedings of the 2015 IEEE/RSJ International Conference on Intelligent Robots and Systems (IROS2015), Hamburg, Germany, 2015, pp. 3862-3868.

[15] S. Yoshihama, et al., "Powder conveyance experiments with peristaltic conveyor using a pneumatic artificial muscle," in: Proceedings of 2016 IEEE International Conference on Advanced Intelligent Mechatronics (AIM2016), Banff, AB, Canada, 2016, pp. 1539-1544.

[16] T. Sato, et al., "An adaptive decentralized control of a serpentine robot based on the discrepancy between body, brain and environment," in: Proceedings of 2010 IEEE International Conference on Robotics and Automation (ICRA2010), Anchorage, AK, USA, 2010, pp. 709-714.

[17] T. Umedachi, et al., "A soft-bodied fluid-driven amoeboid robot inspired by plasmodium of true slime mold," in: Proceedings of 2010 IEEE/RSJ International Conference on Intelligent Robots and Systems (IROS2010), Taipei, Republic of China, 2010, pp. 2401-2406.

[18] R. Adachi, I. Terayama, T. Tanno, T. Hanamura, T. Umedachi, and T. Nakamura, "Initial Study Toward Motion Generation by Autonomous Decentralized Control for Peristaltic Mixing and Conveying Device Imitating Intestines," in: Proceedings of IEEE International Conference on Industrial Technology(ICIT2024), Bristol, UK, 2024, pp. 1-6.

[19] K. Tsurumi, et al., "Generation of Mixing and Transporting Motion for Peristaltic Mixing Pumps by Autonomous Decentralized Control Using Local Feedback with a Discrepancy Function," in: Proceedings of the 51st Annual Conference of the IEEE Industrial Electronics Society (IECON 2025), accepted, 2025.

[20] K. Wakamatsu, et al., "Mixing State Estimation of Peristaltic Continuous Mixing Conveyor with Distributed Sensing System Based on Soft Intestine Motion," in: Proceedings of 2020 3rd IEEE International Conference on Soft Robotics (RoboSoft2020), New Haven, CT, USA, 2020, pp. 208-214.

[21] A. Pikovsky, et al., "Synchronization: A Universal Concept in Nonlinear Sciences," Cambridge, U.K., Cambridge University Press, 2001.

[22] R. Kobayashi, et al., "A design principle of the decentralized control and its applications," in: Proceedings of 11th International Conference on of Numerical Analysis and Applied Mathematics (ICNAAM2013), Rhodes, Greece, 2013, pp. 2440-2443.

[23] T. Umedachi, et al., "True-slime-mould-inspired hydrostatically coupled oscillator system exhibiting versatile behaviors," Bioinspiration & Biomimetics, vol. 8, issue 3, 2013.

[24] T. Umedachi, et al., "Soft-bodied amoeba-inspired robot that switches between qualitatively different behaviors with decentralized stiffness control," International Society for Adaptive Behavior, vol. 23, issue 2, pp. 97-108, Apr. 2015.

[25] D. Owaki, et al., "A quadruped robot exhibiting spontaneous gait transitions from walking to trotting to galloping," Scientific Reports, vol. 7, Mar. 2017.

[26] S. Wang, Y. Li, S. Zhang, B. Wang, and H. Yang, "Relative localization of swarm robotics based on the polar method," International Journal of Advanced Robotic Systems vol. 19, issue 1, Jan. 2022.

[27] V. A. Le and T. X. Nghiem, "Distributed Experiment Design and Control for Multi-agent Systems with Gaussian Processes," in: Proceedings of 2021 60th IEEE Conference on Decision and Control(CDC2021), Austin, TX, USA, 2021, pp. 2226-2231.

[28] A. Lederer, Z. Yang, J. Jiao, and S. Hirche, "Cooperative Control of Uncertain Multiagent Systems via Distributed Gaussian Processes," IEEE Transaction on Automatic Control vol. 68, issue 5, pp. 3091-3098, Sep. 2022.

[29] P. Culbertson and M. Schwager, "Decentralized Adaptive Control for Collaborative Manipulation," in: Proceedings of 2018 IEEE International Conference on Robotics and Automation(ICRA2018), Brisbane, QLD, Australia, 2018, pp. 278-285.

[30] G. Sartoretti, W. Paivine, Y. Shi, Y. Wu, and H. Choset, "Distributed Learning of Decentralized Control Policies for Articulated Mobile Robots," IEEE Transactions on Robotics vol. 35, issue 5, pp. 1109-1122, Jul. 2019.